Turbulence, Combustion and Film Prediction in Rocket Application via Parameter Adjustion, Model Variation and Deep Learning Method

By A.Sternin, H.Ma, J.Liu, O. J.Haidn, AND M.Tajmar†

Institute of Turbomachinery and Flight Propulsion (LTF),
Associate Professorship Space Propulsion,
Technische Universität München (TUM), Boltzmannstraße 15, 85748 Garching b. München, Germany

Our investigations aim at the determination of ranges of reliable applicability of turbulence and turbulence/chemistry interaction models for the case of film cooling in liquid propellant rocket engines. Among the different models investigated have been a Reynolds-Averaged Navier-Stokes (RANS) approach with either k-ϵ or k-ω Reynolds Stress Model (RSM) and an eddy dissipation concept (EDC) with Volume Fraction Constant or the Time Scale Constant (TSC) to account for finite rate kinetics. The final aim is to generate a reliable data base which can be used for supervised machine learning.

1. Introduction

Within the last ten years oxygen/methane has become one of the most promising propellant combinations of the future. All space fairing nations have research programs aiming at preparing a data base for future launcher technologies [1]. Within the SFB-TRR40 several groups contribute experimentally and numerically to this data base [2].

Rocket engines are very specific combustion devices inside which gradients of temperature, velocity, density and species exceed by far those in other combustion chambers. Models which can be successfully used to predict phenomena in standard combustion devices quite often yield erroneous results when applied in rocket engines. As in all combustion devices in rocket engines many different physical phenomena are present but become the dominating one in only a small portion of the combustor. Particularly two regions inside the combustion chamber, the recirculation region downstream of the oxygen post and the wall boundary layer have shown to be extremely import for combustion stability and combustion performance and heat transfer, respectively. While the first defines flame holding and the initial mixing and reactions, the latter is extremely import for wall heat loads [3]. Due to gas temperature which exceed 3000 K at the edge of the boundary layer and wall temperatures around 950 K finite rate chemistry is essential for a reliable heat transfer prediction. Our effort aims at the identification of regions with local dominating processes and of appropriate models suited to describe them reliably.

Wall flows in rocket engines are specific insofar as there is never a fully developed boundary layer and this is even more the case in film cooling applications. In the first

† Institute of Aerospace Engineering (ILR), Technische Universität Dresden (TUD), Marschnerstr. 32, 01307 Dresden, Germany

part of such engines, the acceleration of the flow is a result of the heat release by chemical reactions and further downstream, the flow is additionally accelerated by followed by the converging part of the nozzle. Hence, the near-wall flow is characterised by extremely steep gradients of temperature and velocity which make the application of classical eddy-viscosity turbulence models with the underlying assumption of isotropic stress distribution highly questionable. Therefore, one goal of our research is to compare the results achieved with the k-ϵ model to those achieved with the k-ω RSM approach. As already mentioned there is ample evidence that classical flamelet models yield insufficient wall heat transfer results compared to an EDC approach and therefore an additional goal is to identify the sensitivity of two important parameters of the EDC model, namely the VFC and the TSC. In our deep learning approach, we use a modified convolutional neural network to study the characteristics of film cooling.

2. Experimental Setup and Given Information

Two experimental setups, a capacitive cooled single co-ax injector combustor with square cross section and a five coax injector element thruster with rectangular cross section will be used as guidelines for our numerical approach and for comparison reasons [4, 5]. Both thrusters operate with gaseous oxygen and methane.

2.1. *Single-Element Chamber*

Due to capacitive cooling, combustion chamber pressures and operating time are limited to about 20 bar and 4 seconds, respectively. Optionally, in the first part of the combustor a coolant film can be mounted which allows for film cooling investigations and in addition for the application of optical diagnostic techniques in the near-injector region. The geometrical form and size of this chamber have been chosen to present a sub scale version of a full scale engine. The cross section area of the sub-scale chamber corresponds to a typical surrounding area around an injector element; the contraction ratio of 2.5 which corresponds to a Mach number of 0.25 is typical for modern liquid propellant rocket engines. Meanwhile, it serves as a central test case for the international CFD-community. Experimental parameters are shown in Table 1.

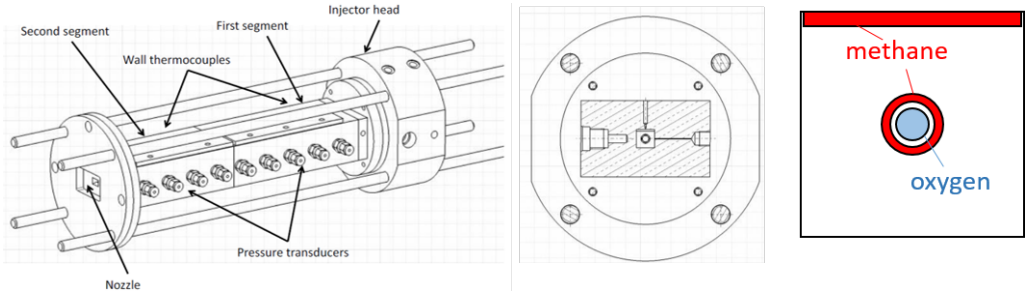

FIGURE 1. Geometry of the LTF-single injector combustion chamber

2.2. *Five-Element Chamber*

In comparison to the single injector hardware, the multi-element combustor is caloric cooled and thus can be operated up to 40 bar combustion chamber pressure. However, the datum experiment aims to expand the knowledge of film cooling systems in

Chamber height	12.00 mm	Mass oxygen injection	23.9 kg/s
Chamber width	12.00 mm	Temperature oxygen injection	268.0 K
Chamber length	310.00 mm	Mass flow methane injection	7.7 Kg/s
Radius oxygen	2.00 mm	Temperature methane injection	275.0 K
Inner radius methane	2.50 mm	Mass flow methane film	2.2 kg/s
Outer radius methane	3.00 mm	Temperature methane film	266.0 K
Height of film slot	0.25 mm	ROF	3.1
		Chamber pressure	10.0 bar

TABLE 1. Geometry of the LTF-single injector combustion chamber.

methane/oxygen engines, which have a pressure level of 2MPa, typical for small upper stage engines.

The multi-injector chamber with film applicator is depicted in 2. From the interface between the first and second segment, the coolant film is injected into the chamber, i.e., the coolant film only protects the second segment of the chamber.

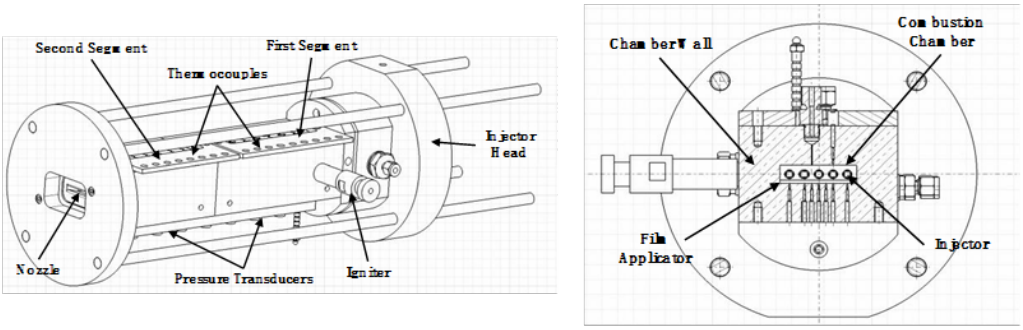

FIGURE 2. Geometry of 5-el. Combustion chamber

3. Numerical Approach and Methodology

Our investigations aim at the determination of models for turbulence and turbulence chemistry interaction applied to combustion devices of liquid propellant rocket engines. In a first approach we investigate the applicability of a standard k-ϵ approach with a ω-RSM one, then we investigate the impact of parameters of the EDC approach for the case of film cooling of a rocket engine and finally we check the suitability of a deep learning approach for such a cooling flow.

3.1. *RSM Turbulence Model setup*

The omega-based BSL-RSM-Model was chosen as it revealed to be the most stable among the RSM models and with the best convergence. Omega transport equation in eq. 3.1. The RSM transport equation is depicted in eq. 3.2 with distinction between terms with modelled components (green) and those without (blue)

$$\frac{\delta}{\delta t}(\rho\omega) + \frac{\delta}{\delta x_j}(\rho\omega u_j) = \frac{\delta}{\delta x_j}\left(\Gamma_\omega \frac{\delta\omega}{\delta x_j}\right) + G_\omega - Y_\omega + D_\omega, \tag{3.1}$$

$$\begin{aligned}\frac{\partial}{\partial t}(\rho\overline{u_i'u_j'}) \quad &+\frac{\partial}{\partial x_k}\left(\rho u_k\overline{u_i'u_j'}\right) = -\frac{\partial}{\partial x_k}\left[\rho\overline{u_i'u_j'u_k'}+\overline{p'}\left(\delta_{kj}u_i'+\delta_{ik}u_j'\right)\right] \\ &+\frac{\partial}{\partial x_k}\left[\mu\frac{\partial}{\partial x_k}(\overline{u_i'u_j'})\right] \\ &-\rho\left(\overline{u_i'u_k'}\frac{\partial u_j}{\partial x_k}+\overline{u_j'u_k'}\frac{\partial u_i}{\partial x_k}\right) \\ &-\rho\beta\left(g_i\overline{u_j'\theta}+g_j\overline{u_i'\theta}\right) \\ &+p'\left(\frac{\partial u_i'}{\partial x_j}+\frac{\partial u_j'}{\partial x_i}\right) \\ &-2\mu\frac{\overline{\partial u_i'}}{\partial x_k}\frac{\partial u_j'}{\partial x_k} \\ &-2p\Omega_k\left(\overline{u_j'u_m'}\varepsilon_{ikm}+\overline{u_i'u_m'}\varepsilon_{jkm}\right).\end{aligned} \tag{3.2}$$

For comparison with eddy viscosity (EV) Models a reverse derivation of characteristic turbulence properties is possible. Dissipation rate ϵ is calculated from transported specific dissipation rate ω

$$\epsilon_{ij} = \frac{2}{3}\delta_{ij}\rho\beta^*_{RSM}k\omega \tag{3.3}$$

The turbulent kinetic energy k is modelled directly from the transported RST

$$k = \frac{1}{2}\overline{u_i'u_i'}. \tag{3.4}$$

Turbulent viscosity μ_t is calculated from k, ϵ and the density ρ

$$\mu_t = \rho C_\mu\frac{k^2}{\epsilon}. \tag{3.5}$$

The RSM results will be compared with standard k-epsilon results.

$$\frac{\delta}{\delta t}(\rho k)+\frac{\delta}{\delta x_i}(\rho k u_i) = \frac{\delta}{\delta x_j}\left[\left(\mu+\frac{\mu_t}{\sigma_k}\right)\frac{\delta k}{\delta x_j}\right]+G_k+G_b-\rho\epsilon-Y_M \tag{3.6}$$

$$\frac{\delta}{\delta t}(\rho\epsilon)+\frac{\delta}{\delta x_i}(\rho\epsilon u_i) = \frac{\delta}{\delta x_j}\left[\left(\mu+\frac{\mu_t}{\sigma_\epsilon}\right)\frac{\delta\epsilon}{\delta x_j}\right]+C_{1\epsilon}\frac{\epsilon}{k}(G_k+C_{3\epsilon}G_b)-C_{2\epsilon}\rho\frac{\epsilon^2}{k} \tag{3.7}$$

This study aims at the single-element combustion chamber but with the following simplifications: The combustion products enter the combustor at frozen equilibrium conditions for a mixture ratio of 3.1, the film is injected at the same position on the top of thruster; see Figure 3. The list of species considered for the mixture origins in the work of Slavinskaya [12]. The temperatures of the hot gases and the film are 3326 K and 266 K, respectively. Because this simplification is solely used to investigate the effect of turbulence models, no reactions are modelled, just turbulent and diffusive species transport.

The simulation cases include the right half of the simplified chamber where the “symmetry plane” over the x and y coordinate (at z=0) serves as the left “symmetry” boundary condition. Since the literature on applications of the RSM approach for rocket engines is scarce, a step by step methodology has been chosen. In order to distinguish between the influence of boundaries, edges and gradients on secondary flow phenomena, a second mesh was created, where the right wall was replaced by another symmetry pane

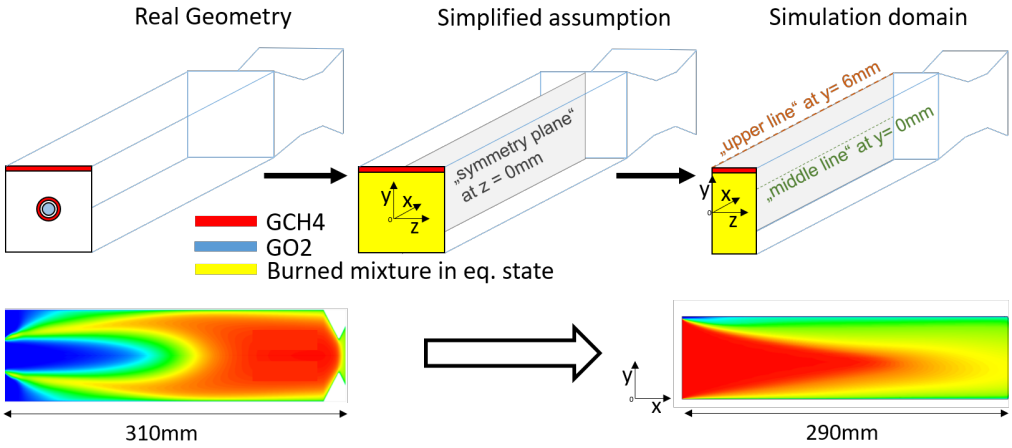

FIGURE 3. Simplification of the single-element combustion chamber

(Figure 4). In this way a 2D-Condition was created. The absence of a nozzle served the purpose of almost equal pressure conditions. Due to the simplicity of the cases, very clear and direct conclusions can be made about specific model and flow characteristics. ANSYS Fluent 18.0 was used.

Upper boundary	No slip wall (adiabat, 260K, temperature gradient)
Low boundary	No slip wall (adiabat, 260K)
right boundary	No slip wall (adiabat, 260K) , symmetry
left boundary	symmetry
Outlet	Pressure outlet 10bar
Inlet Mixture	Mass flux to reach the mass flow from the experiment (OX+CH4), 3326.54K (=Eq. Temp. at 10bar), Species Mixture in the equilibrium state (no CH4 for better film mixing indication)
Inlet Film	Mass flux to reach the mass flow from the experiment, 266K
Turbulence Models	K-Epsilon, K-Omega-BLS-RSM
Pr/Sc	0.9/0.6
Turbulence production limiter	none
Pseudo-CFL (in steady state)	1
Spacial discretisations	Second order
Reached residuals	$<10^{-8}$

TABLE 2. Simulation setup and its variations

As shown in Table 2, the upper, right and lower wall boundary conditions as well the turbulence model have been varied; see Table 3.1 for each set of conditions for the simulation cases. The abbreviations will be used further for identification.
Before each abbreviation additionally “RSM”, or “k-ϵ” will be placed to indicate the used turbulence model.
“M1” in the abbreviation stands for all cases with Mesh 1 used (figure 4) when the right boundary is a wall according to the experiment.

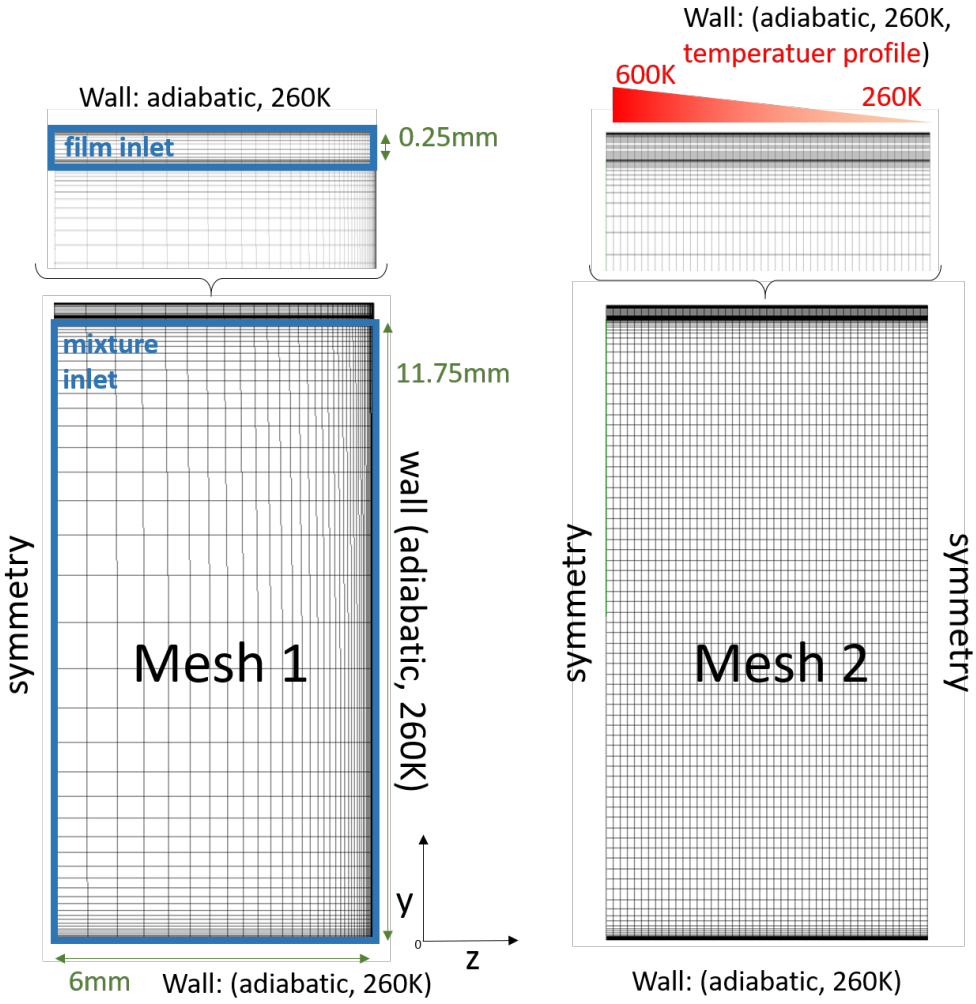

FIGURE 4. Spatial discretisation of the simplified geometry; Mesh 1: Standard Mesh of the simplified case. Mesh 2: Same case but with right wall also as symmetry for a 2D-Flow-Condition

"M2" stands for all cases with Mesh 2 used (Figure 4) where the right boundary is replaced by a symmetry plane and aim at suppressing the wall influence.
"Adi" means , that all walls are adiabatic. "Top" means that only the upper wall is non-adiabatic but has a constant temperature of 260 K. "Top-Grad" stands for a Temperature profile at the upper wall. "Top-Right" means that only the lower wall remains adiabatic while the upper and right wall have a constant temperature and "All" means that all walls have the constant temperature of 260 K. The ending "NF" means that no film is injected.

3.2. *EDC Model and Variation strategy*

The EDC model is derived from the consideration that since chemical reactions take place exclusively on molecular length scales (ν) their interaction with turbulence occurs only through small Kolmogorov-Eddies. Using assumptions about the turbulent cascade from Spalding and Kolmogorov [7, 8] a mathematical connection between ν-turbulence

Case abbreviation	**Condition**
M2-Top	Mesh 2, right boundary as symmetry, 260K at upper wall, adiabatic lower wall
M2-Top-Grad	Mesh 2, right boundary as symmetry, uneven temperature distribution at upper wall (linearly from 600K at left symmetry to 260K at right symmetry, constant in main stream direction), adiabatic lower wall
M1-Adi	Mesh 1, right boundary as wall, adiabatic upper wall, adiabatic right wall, adiabatic lower wall
M1-Top	Mesh 1, right boundary as wall, upper wall 260K, adiabatic right wall, adiabatic lower wall
M1-Top-Right	Mesh 1, right boundary as wall, upper wall 260K, right wall 260K, adiabatic lower wall
M1-All	Mesh 1, right boundary as wall, upper wall 260K, right wall 260K, lower wall 260K
M1-Adi-NF	Mesh 1, right boundary as wall, adiabatic upper wall, adiabatic right wall, adiabatic lower wall, film mass flow = 0
M1-All-NF	Mesh 1, right boundary as wall, upper wall 260K, right wall 260K, lower wall 260K, film mass flow = 0

TABLE 3. Simulation cases and their conditions

and it's one-way energy exchange with the chemical field can be derived

$$w^n = \frac{3}{2} C_{D1} \frac{u^n}{L^n} \left(u^n\right)^2 \tag{3.8}$$

$$q^n = C_{D2} \nu \left(\frac{u^n}{L^n}\right)^2 \tag{3.9}$$

$$\gamma_\lambda^* = \left(\frac{3C_{D2}}{4C_{D1}^2}\right)^{\frac{1}{4}} \left(\frac{\nu\epsilon}{k^2}\right)^{\frac{1}{4}} = C_\gamma \left(\frac{\nu\epsilon}{k^2}\right)^{\frac{1}{4}} \tag{3.10}$$

$$\tau_\lambda^* = \left(\frac{C_{D2}}{3}\right)^{\frac{1}{2}} \left(\frac{\nu}{\epsilon}\right)^{\frac{1}{2}} = C_\tau \left(\frac{\nu}{\epsilon}\right)^{\frac{1}{2}}. \tag{3.11}$$

q^n is the dissipative energy loss of turbulent cascade level n. w^n is the transport of energy from cascade n-1 into cascade n. The constants C_{D1} and C_{D2} regulate the relation of those transports. According to this theory a variation of one of those constants would result in a strong variation of viscosity and secondary a variation of the relation $\frac{u^n}{L^n}$ where u^n is the velocity and L^n the length scale of the cascade level n. * marks the smallest turbulent scale.

This fine structure is assumed to host the reactions in form of an adiabatic perfectly stirred reactor (PSR). Connecting that with further models for turbulent flame front a mathematical correction term for chemical reaction rates has been derived

$$\dot{R}_i = \frac{\rho}{\tau_\lambda^*} \frac{\gamma_\lambda^{*2}}{\left(1 - \gamma_\lambda^{*3}\right)} \left(Y_i^* - Y_i\right). \tag{3.12}$$

C_γ is the volume fraction constant (VFC) and C_τ the time scale constant (TSC). Y_i is the mass fraction of species i and Y_i^* its mass fraction after reaction time τ_λ^*. This Formula is implemented in ANSYS Fluent 18.0 which was used in this work.

In order to asses the impact of variations of the EDC-parameter VFC and TSC, the following studies have been performed, see table 4. The first variation (TSC-Var) aims at the TSC. The second variation (VFC-Var) only changes the VFC against the default case (DEF). Here only C_{D1} but not C_{D2} is varied. The third variation (TSC-VFC-Var) is aiming to observe a change exclusively in C_{D2} against DEF. The numerical response of the system will be observed. The values have been chosen, based on previously gained experience [9].

	TSC	VFC	C_{D1}	C_{D2}
Default values (DEF)	0.4082	2.1377	0.1340	0.5
Var. 1 (TSC-Var)	3.0	2.1377	0.9847	27.0
Var. 2 (VFC-Var)	0.4082	10.0	0.0061	0.5
Var. 3 (TSC-VFC-Var)	3.0	5.7952	0.1340	27.0

TABLE 4. EDC Parameter Variations

As already mentioned, the study aims at the single-element combustion chamber. The domain was reduced to two dimensions since only the interior operational conditions are the decisive factors here. The domain ends before the nozzle for comparable, pressure-independent results.

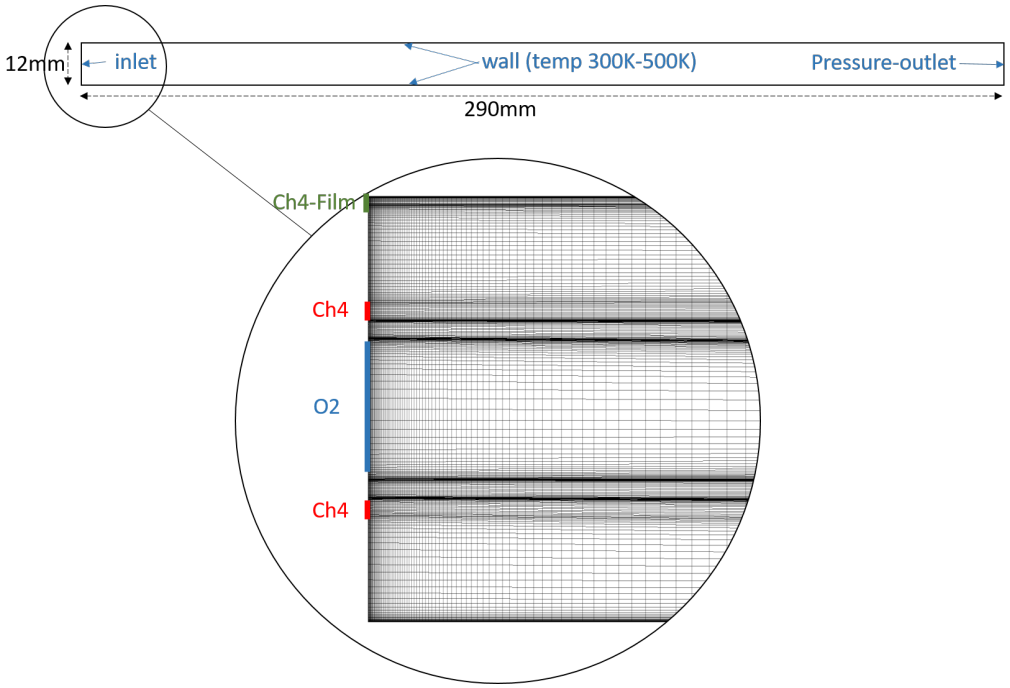

FIGURE 5. 2D-Mesh along the chamber with cut nozzle

3.3. *Deep Learning Method*

The study using deep learning method aims at the five-element combustion chamber experiments, as described in subsection 2.2. Similar to the RSM approach in subsection

3.1 and shown in Figure 3, the coaxial injection of the experiment is not modelled in order to reduce the computational costs of the simulation procedure. The components of the gas mixture are calculated using the temperature-pressure-problem module of CEA. The equilibrium temperature of the main gas is 3326 K. The RANS-k-ϵ solution calculated by ANSYS Fluent focuses on the mixing characteristics of the methane film cooling. Hence, chemical reactions were not considered here.

The mass fluxes of main gas and coolant film in the CFD simulation are chosen as random values, shown in Table 5, which are beneficial for the following training work. And the temperatures of the coolant are evenly distributed as six values in the range between 200 K and 300 K.

Variables	Unit	Range	Amount	Values
$\dot{m}_m$	$kg/(m^2 \cdot S)$	$140 - 400$	196	random
$\dot{m}_c$	$kg/(m^2 \cdot S)$	$550 - 1200$	196	random
T_c	K	$200 - 300$	6	200,220,240,260,280,300

TABLE 5. Simulation campaign

In order to indicate the characteristics of mixing in both dimensions, the learning region is resampled onto regular 64×256 grids to obtain the ground truth data sets including inputs and targets. The inputs, including mass fluxes and coolant temperature, are rearranged as initial fields, meanwhile, the simulation results of each case are interpolated into a set of rectangular matrices with the same size. The value in every row of the inputs initial field describes the mass fluxes and temperature. The assumption is that there is a boundary row in the matrices whose values describe the boundary between main gas stream and coolant film accurately. The targets include 16 items: both x and y components of velocity, pressure, and concentrations of the 12 gaseous species for both hot gas mixture and coolant film. The first four channels contain the flow field information including x and y velocity components, pressure, and temperature sequentially. The next twelve channels contain the concentration of every species from mainstream and coolant film.

Nondimensionalisation is a normal data processing method in numerical calculation of fluid mechanics by which the features with different properties can be compared. We can obtain dimensionless quantities using the corresponding characteristic quantity. In addition, mean pressure is subtracted from every dimensionless pressure. Lastly, the values of the matrix in each channel are normalised to the [–1,1] range in order to minimise errors in the training phase. Both inputs and targets matrices are processed by this method. The data pre-processing method can flatten the training space and simplify the training task using the deep neural network, resulting in the acceleration of the convergence speed.

The neural network in this paper is based on one U-net architecture, which is widely used in the field of machine vision. By means of convolutional calculation, the features are extracted from the original data set.

At the beginning of the convolutional neural network (CNN) architecture illustrated in Figure 6, mainstream mass flux, coolant film mass flux, and coolant temperature from the data set are introduced into the architecture as three rectangular matrices whose size is 64×256.

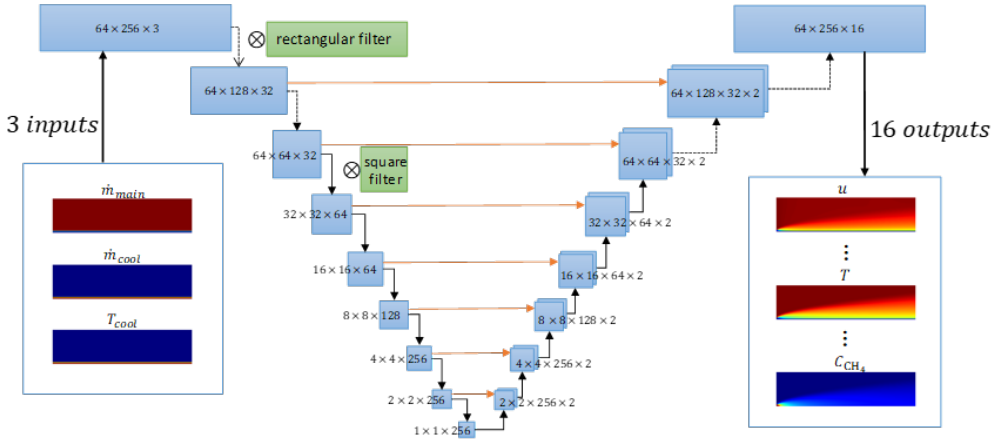

FIGURE 6. Schematic of U-net architecture

In the training process, the weights of every convolutional blocks are optimised by the means of backpropagation, which need one loss function to calculate the difference between results and ground truth. For supervised training, a basic loss function can be defined as

$$L = \sum_{i=1}^{I} \sum_{n=1}^{N} |X_{out} - X_{tar}| , \tag{3.13}$$

where I = target amount; meanwhile N = batch size denotes the number of cases used in the CNN architecture in one batch operation.

4. Result Analysis

4.1. *Trade-Off Comparison between RSM and k-ϵ*

In this sub-chapter the effects of the switch from the k-ϵ to the RSM turbulence model are traced. At first the symmetrical cases on Mesh 2 are compared in order to distinguish between vertical and horizontal flow characteristics. Then step by step switches from adiabatic conditions to equally heated walls are analysed. The emphasis here lies on the individual role of each cross recirculation in form of lateral swirls. Finally, the k-ϵ and the RSM cases are evaluated in terms of heat protection capability of the film. Longitudinal plots are always located on the vertical “symmetry plane” over the y- and z-coordinate (at z=0) in the chamber. (see Figure 3)

4.1.1. *Comparison between : k-ϵ-M2-Top, RSM-M2-Top, k-ϵ-M2-Top-Grad, RSM-M2-Top-Grad*

Very clearly observable in Figure 7 is a difference in the Eddy-Viscosity (EV) production between RSM and k-ϵ. While k-ϵ produces more EV along the walls, RSM EV production is higher in the shear layer between film and main flow. That matches with previous experience according to which the k-ϵ model tends to overestimate the turbulence production in the near wall region while the k-ω model under estimates it in regions of higher Reynolds number. The RSM results show here a downwards correction of the near wall EV and an upwards correction in the free stream area against the k-ϵ. The film-TKE in the k-ϵ case starts with a relatively high fixed value, given as a required boundary

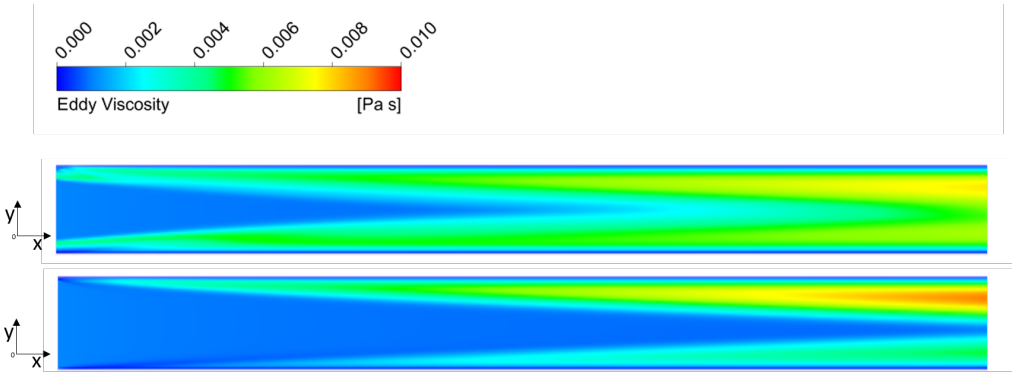

FIGURE 7. Eddy Viscosity contour, k-ϵ-M2-Top (upper), RSM-M2-Top (lower)

condition. Thus, the positive correction in RSM is noticeable only further downstream in the shear layer.

RSM solves the problem to bypass the gap between limits of the k-ϵ and k-ω model. The for this purpose usually used k-ω-SST has been ruled out in previous work [6]. Its blending function is derived from very generic flow pattern and did not perform sufficiently in the given condition.

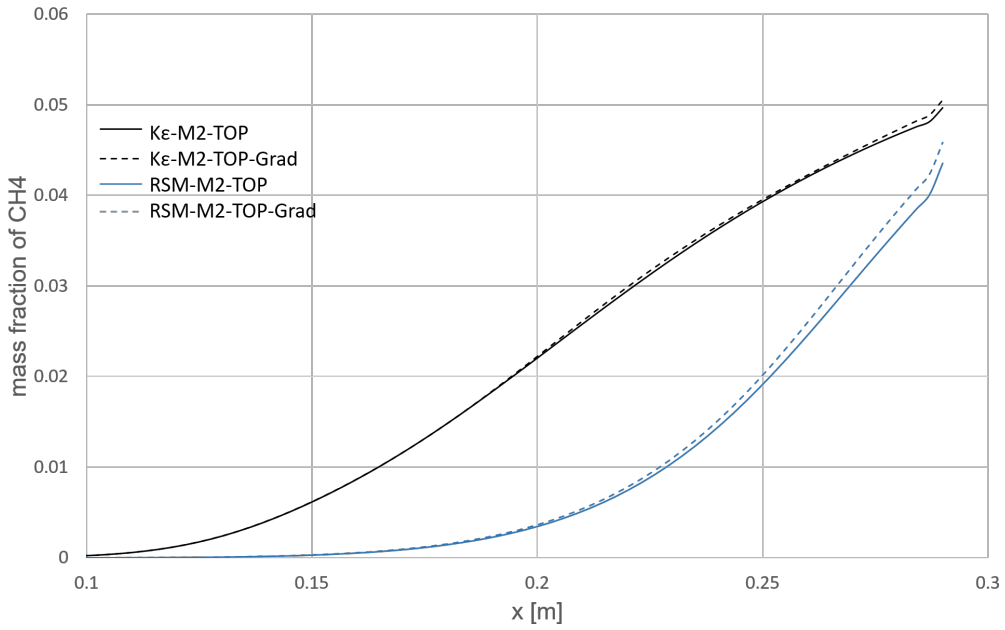

FIGURE 8. CH4 mass fraction along the middle line x-direction on the symmetry plane

Several observations can be made by plotting the CH4 mass fraction along the middle axis, solid and dashed lines in Figure 8. In the first 220mm the EV incline in k-ϵ-cases is higher but relatively constant while the RSM graphs show a raising inclination over x. This is coherent with the different observations of the EV production in Figure 7. Due to the overall overestimation of the EV by k-ϵ, the stronger turbulent mixing transports more

film material (CH4) to the centre. Further downstream, the mixing by the secondary flow is building up and becoming the dominant driving force for mixing. The graphs suggest that in a longer tube, further downstream the CH4.-mixing in RSM would exceed the one in k-ϵ.
The dashed lines in this figure allow a comparison of the results achieved with constant temperature boundary condition of at the upper wall (M2-Top) and with a temperature gradient in Z-direction from 600K at the middle plane to 260K on the right (M2-Top-Grad). Similar gradients appear also in experiments where the wall temperature is decreasing from a centre maximum towards the edges. Because of the symmetry condition of the right boundary the only possible secondary flow can origin solely from the inhomogeneous temperature boundary condition. The RSM case with the temperature gradient (RSM-M2-Top-Grad) provides a slightly better mixing. The reason for that is that the higher temperature on the left side of the upper wall results in a stronger thermal expansion of the film than on the right. That provokes a recirculation in cross direction to the flow. However, the velocity of this particular secondary effect is below 0.3% of the main stream velocity. Nevertheless, in terms of species distribution in different parts of the domain the difference can be up to 15%.

4.1.2. *Comparison between: RSM-M1-Adi, RSM-M1-Top, RSM-M1-Top-Right, RSM-M1-All*

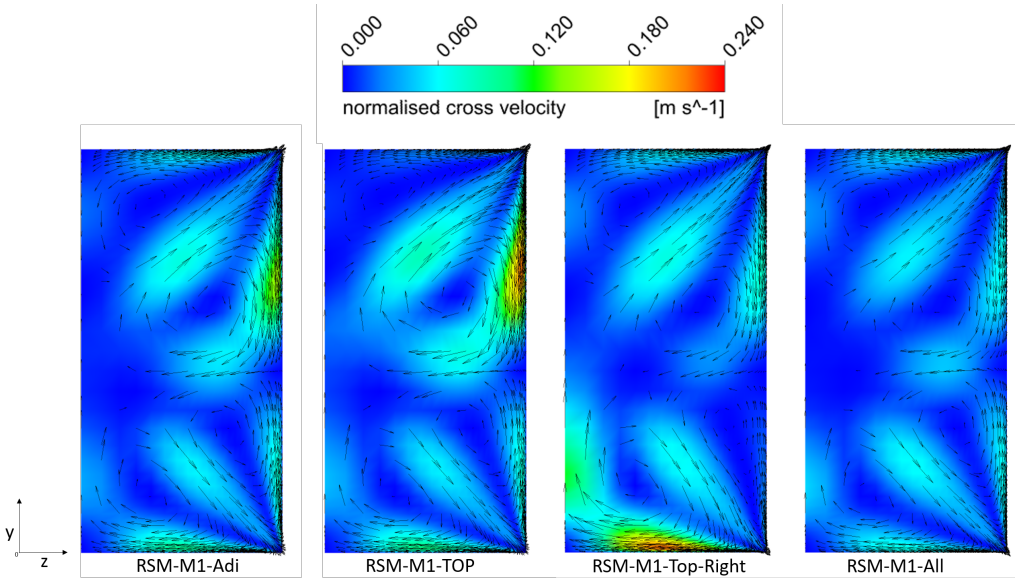

FIGURE 9. Lateral flow velocity and lateral flow vectors at x=200mm

Coming back to Mesh1 with the no-slip wall condition at the right boundary, a step-by step switch from an adiabatic condition to one with constant wall temperatures is depicted in Figure 9. The lateral swirls represent a “secondary flow of the second kind”. It is driven by Reynolds stress gradients in lateral direction [10,11]. Two main vortex pairs according to the tube flow theory can be seen. While the upper one transports mainly film material along the side wall downstream towards the lower pair where the main path of transport is oriented towards regions further down. Activating the wall cooling

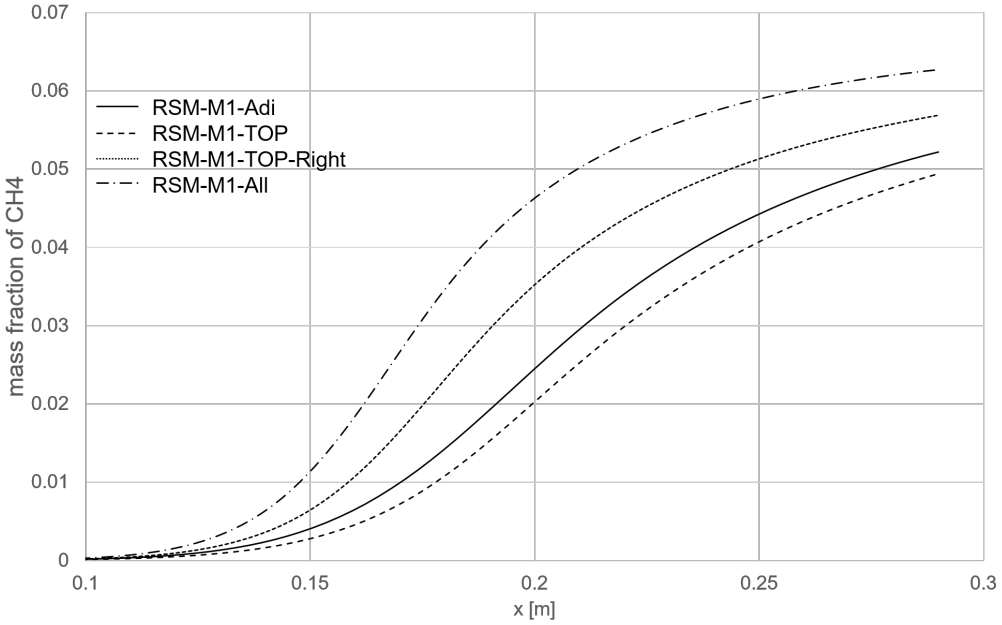

FIGURE 10. CH4 mass fraction along the middle line in x-direction on the symmetry plane

step by step results in a specific impact on the four swirls. In the adiabatic case (RSM-M1-Adi) cross flow is mainly induced by Reynolds stress gradients towards the corner regions as well as the shear between the film and the main flow. After switching on the cooling on one wall after an other, the flow patterns respond in two opposed ways. The energy evacuation from the respective boundary layer slows down the closest swirl impairing its particular function. Simultaneously, the stronger temperature and density gradient produces additional Reynolds stresses which stirs the angular momentum in close region. This second effect is inferior to the first one but influences a wider area.

The switch of the upper wall from adiabatic condition to constant temperature (RSM-M1-TOP) leads to a weakening of the upper swirl. Hence, the transport of the film material decreases by ca. 5%. While the additional Reynolds stresses can't compensate for it, they boost the neighbouring swirl. Setting the right wall to 260K (RSM-M1-TOP-Right) results in additional heat sink and leads to the asymmetrical film heating as investigated in subchapter 4.1.1. Hence the the methane transport away from the top wall is promoted again by 15.2%. This magnitude is much higher than in the previous symmetrical M2-cases (Figure 8) due to additional Reynolds stress gradients in the non-isotropic geometry. Analogous to the previous steps a heat sink at the bottom wall (RSM-M1-All) withdraws energy from the lower recirculation and hence impairs its capability of evacuating CH4 from the middle height to the lower regions. This results in a 10% higher mass fraction there. That goes together with an increase of Reynolds stresses. Figure 10 tracks the methane mass fraction along the middle line (its position is shown in Figure 3).

The magnitude of Reynolds stress gradient driven cross recirculation (swirls) is accumulated with each heat sink, and finally influence the entire cross section. Hence, in a fully cooled chamber, the impact is rather dominant near the symmetry plane where it contributes to the intermixing of the film. Closer to the side walls primary the energy

withdraw impairs the angular momentum of the swirls and hence the destabilising mechanisms for the film. In the cases with all walls cooled (RSM-M1-All) secondary velocities reach in near wall regions 10% of the velocities in main stream direction (x). But also in the middle region values of 6% relative cross velocity are eminent.

4.1.3. *Comparison: k-ϵ-M1-All, RSM-M1-All, k-ϵ-M1-Adi, RSM-M1-Adi, RSM-M1-All-NF*

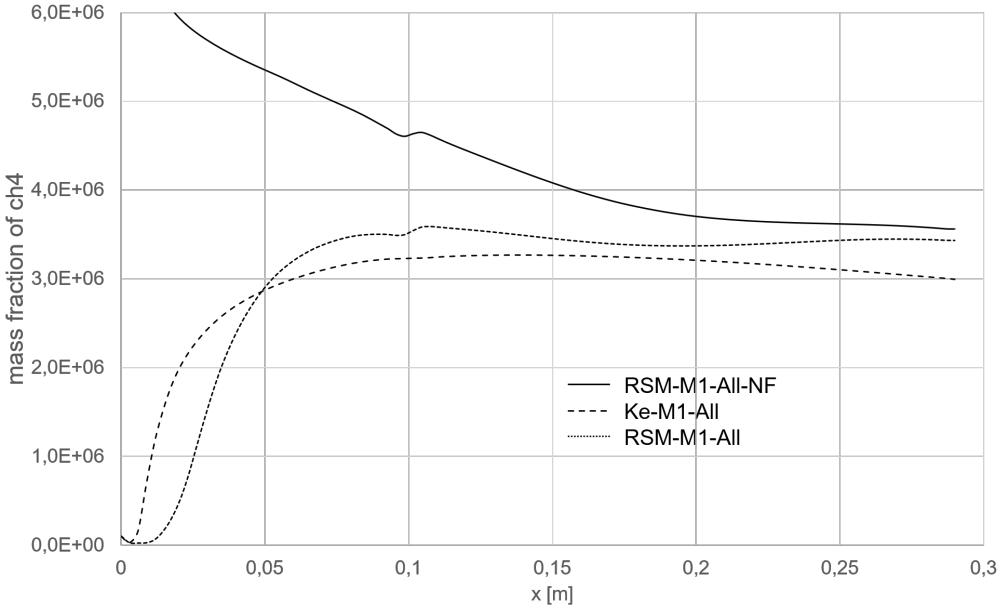

FIGURE 11. Wall heat flux along the upper line in x-direction on the symmetry plane

Finally, the wall heat fluxes are compared, see Figure 11 which shows the heat flux values achieved with the k-ϵ, RSM approaches together with the reference case of no film cooling. While the k-ϵ approach yields initially higher heat fluxes due to stronger near wall eddy viscosities, cross flows established further downstream become the driving force of the convection and therefore the RSM predicts higher heat fluxes than the k-ϵ already about 0.05 m downstream of the face plate. Both approaches predict no further heat flux increase for downstream positions larger than 0.15m although a comparison with the reference case still shows some small cooling effect of the film. This is due to energy absorption by the walls. While the k-ϵ approach has limited capabilities to account for this counteraction, the RSM approach reacts to this additional free shear layer and the resulting production of eddy viscosity kicks in at x=0.2 m. The stronger turbulent mixing of the film conveys additional hot gas to the wall which leads to a slight enhancement of the wall heat loads along a short length until x=0.27 m. Overall, the RSM approach (RSM-M1-All) tends towards wall heat flux values similar to the reference ones (RSM-M1-All-NF) but doesn't reach them.

4.2. *Sensitivity Analysis of TSC and VFC Variations*

In this subchapter the system response to a variation of the EDC parameter is analysed. Figure 12 shows the temperature distribution in the used 2D-domain. On the left side the propellants are injected as described in the experimental setup in subsection 2.1. In the

wake of the central tube a small but stable recirculation zone is functioning as a flame holder. It conserves its energy by regularly retrieving reactants from its environment and producing through their chemical reaction. This process builds the root of the reacting shear layer further downstream. Within the entire length of the combustion chamber the reacting flow is highly disturbed and does not fit to any generic assumption based on tube flows. Since the turbulence coupled EDC model bases on such assumptions as explained in subsection 3.2 its parameters require a reconsideration. Figure 12 shows the response of the system to three specific changes of those parameters. In the following the character of this response is analysed.

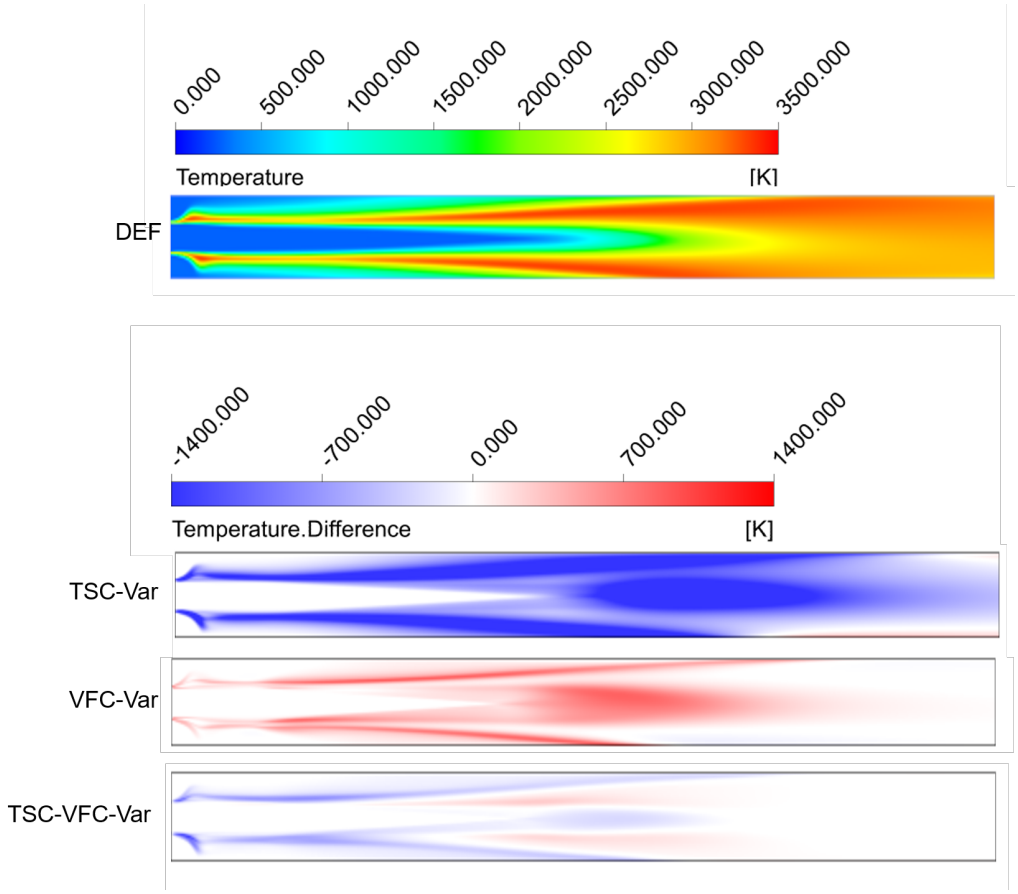

FIGURE 12. 2D-temperature-contours in flow direction in reference case and variation cases

Reduction of TSC (TSC-Var) slows down the reaction rates and hence the produced heat. This can be expected from the implementation of the TSC in the denominator of the fraction which corrects the reaction rates. This change mainly influences the reaction rates but not the equilibrium composition of the reactants. Therefore, a slowed down (TSC-Var) and accelerated (VFC-Var) combustion process, respectively, shifts and stretches the flame front. This is indicated by the negative or positive difference plots in Figure 12. Nevertheless, further downstream this difference to the results of the standard setting is reduced towards zero. The same reason leads to a slightly positive (TSC-Var) and negative (VFC-Var) temperature difference, respectively, in the near wall

regions downstream. In the reference case (DEF) the cold walls withdraw more energy from the flow, because the hot flame reaches the near wall region earlier.

VFC is implemented in the numerator as well as in the denominator of the correction fraction in the EDC model. However, it is negative in the denominator. Accordingly, the reaction rates rise in the "VFC-Var" case. In a hypothetical case of e.g. very low density, the stronger ratio between kinetic viscosity and turbulent dissipation would result according to the EDC model in slower or even inverted reactions. Also a much higher VFC would have this effect. But this scenario would be nonphysical and not expected or considered for these applications.

In the "TSC-VFC-Var" case both, the TSC and the VFC are increased. Neither an exclusively global increase nor a decrease of reaction speed can be seen. Depending on the local flow characteristics, different regions respond in individually. The maximum hot gas temperature does not change. Its value of around 3490K corresponds to the equilibrium temperature of the overall oxygen-methane-mixture (ROF). The reaction rates are getting weaker in the outer parts of the flame and increased inside. The result is that the reactive shear layer is quenched. This case states a numerical combination of the variations before (TSC-Var, VFC-Var). The acceleration and deceleration of the reactions are balanced between each other depending on the relation between local TKE, ϵ, and viscosity. According to the model theory the influence of this balance depends mainly on the kinematic viscosity. This becomes in fact higher towards the center of the reactive shear layer. This effect disappears downstream behind the main mixing region.

Overall it can be concluded, that the connection between turbulence and chemistry is sensitive and interactive since the different flame patterns also influence the viscosity and eddy viscosity evolution. Although in EDC-theory only turbulence-to-chemistry effect is considered, the high gradients in a rocket chamber combustion chamber create a backward information flow from chemistry to turbulence. Changes in temperature and density gradients produce different shear stresses. Their influence on secondary flows as described in subsection 4.1 create complex co-dependency between the combustion and turbulence model.

4.3. *Learning Results*

The baseline case ($m_m = 240kg/\left(m^2 \cdot S\right)$, $m_c = 800kg/\left(m^2 \cdot S\right)$,$T_c = 260K$) describes the film cooling setup which has been investigated previously [13]. After the current initial learning phase, the experimental data will be used in addition to RANS simulations to train the CNN method for film cooling including chemical reactions.

Comparisons between RANS results and learning results are shown in 13. In general, the trained neural networks results are almost the same with RANS results and only in the vicinity of film applicator larger deviations of the flow field are visible which are a result of differences in the predicted y velocity components (Figure 13 (b)). Nevertheless, the overall trend about the concentration distribution of species is predicted fairly well.

5. Conclusion

From the findings of the simplified "preburned" cases, it can be concluded, that the k-ϵ-produced eddy viscosity tends to exceed the one derived from the RST in the RSM case. Cross flow effects occur in the magnitude of 6–10%. They consist mainly of "secondary flows of second kind", as called by Prandtl. Those Reynolds stress gradient-driven velocities grow stronger by the additional anisotropy produced by wall cooling. Other influences on the cross flows are temperature/velocity gradients between film and

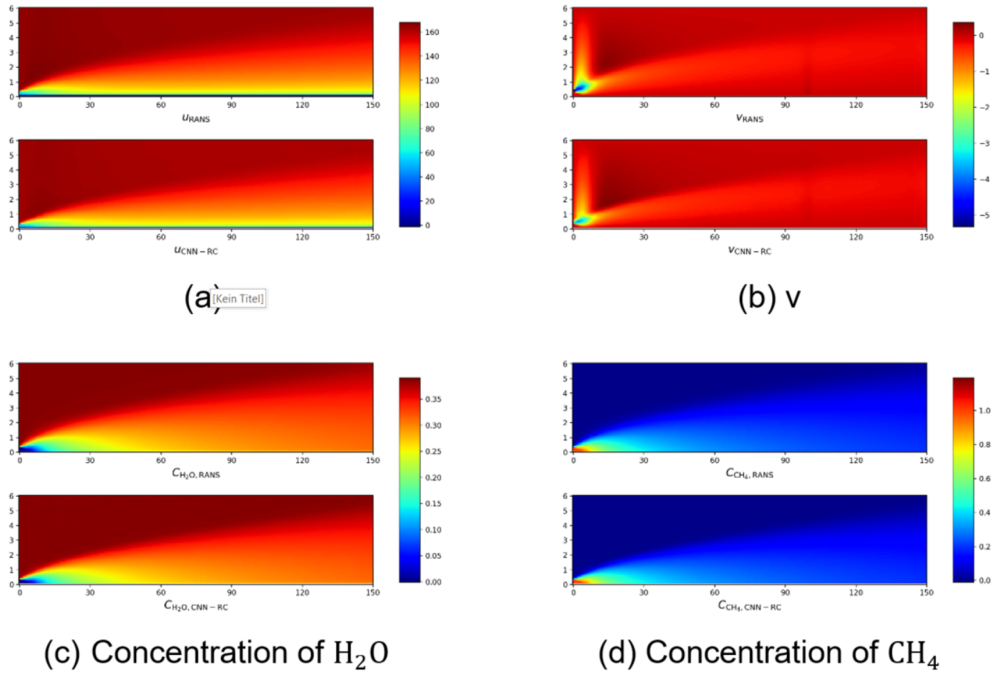

FIGURE 13. Comparison between RANS results and CNN results

hot flow, uneven near wall diffusion processes and the uneven film expansion due to the stronger cooling at the edges. Still, RSM considered secondary flow as swirls can make the difference between a steep and a flat wall heat flux distribution or have other crucial influence on mixing driven phenomena such as species redistribution.

In the frame of previous summer programs conclusions about a realistic EV-distribution and Pr/Sc- adjustments have been made for linear 2-eq-models by validating wall heat fluxes and pressure distribution. As seen in this work the “new” factor in form of cross flows can provide substantial additional mixing potential and even overcome a lower EV production. Assuming that the RSM model naturally provides a more dependable representation of flow patterns it is recommended to investigate further if it can replace linear models for such applications. In this case the suitability of the currently used Pr_t/ Sc_t should be corrected for the RST approach. For that and other reasons a simulation with resolved injectors is currently in production. Also alternatives as quadratic k-ϵ model and EARSM will be investigated. Since the measurement accuracy and resolution are limited, enhanced validation strategies such as indirect measurement and high-fidelity simulations will be consulted. However, it is difficult to believe that demands for a reliable RANS-prediction, especially in terms of the interaction between turbulence and volumetric reactions can be satisfied without using a non-linear turbulence model.

Similar to finding and adjusting an appropriate turbulence model, choosing a suitable chemical kinetic model is crucial for reliable RANS-based combustion simulations. EDC Parameters have a strong influence on the reaction rates in different manners due to different flow conditions in the chamber. Reaction rates may be globally increased and decreased and even quenching may be initiated. The flow field however reacts quite sensitive to the differently produced local energy. Especially in terms of molecular and

turbulent viscosity. This makes the optimisation problem between turbulence and combustion model adaption a multidimensional one.

Strong gradients (up to 1000 K/mm) in the reactive shear layer and boundary layer create a backward influence from the turbulence-affected reactions to the turbulence itself. This sensitive feedback occurs in length scales corresponding to the flow field gradients. It is expected that this reciprocal correlation is happening on each level of the turbulence cascade. Hence, the assumptions about canonical eddy breakup processes may not be entirely applicable in such strongly disturbed environment. A possible improvement could be an empirical EDC parameter adjustment. In that case the change of the parameters would compensate for any possible inaccurate assumptions about the turbulence phenomenon. This solution would be rather restricted in operational conditions. A further extension can be corrections of the turbulence model itself where the additional feedback from chemistry to turbulence is implemented in a more flexible way. The complex co-dependencies between turbulence and chemistry also state a challenge for data driven approaches. Especially the supervision strategies in deep learning methods have to take this complexity into account.

Finally, a method for using convolutional neural networks to directly predict the mixing characteristics between coolant film and hot non-reacting gases is presented. The training data for the supervised learning is obtained from RANS simulations. A U-net architecture is modified to encode and decode features of the flow field. The modified architecture and related learning settings are implemented to baseline and test cases, and get the results which have less than 0.55% global errors. This work has presented a study that utilises a machine learning approach to directly get the solutions about film cooling in rocket combustion chambers, when given the inlet flow conditions. The work proved the practicability that convolutional neural networks solve the multiple flows mixing problem by the means of supervised learning with small sample set. While the work presented is based on the RANS solutions, the modified neural network architecture is generic, and can be applied to a wide range of partial differential equation problems in rectangular Cartesian coordinate system.

Acknowledgements

Financial support has been provided by the German Research Foundation (Deutsche Forschungsgemeinschaft – DFG) in the framework of the Sonderforschungsbereich Transregio 40.

References

[1] SILVESTRI, S., BAUER, C., LUNGU, P. AND HAIDN, O. (2018). Axial and azimuthal heat load distribution in 7-injector GOX/GCH4 combustion chamber. In: *Proceedings of the 54nd AIAA/SAE/ASEE Joint Propulsion Conference*. Cincinnati, USA.

[2] HAIDN, O., ADAMS, N., RADESPIEL, R., SCHRÖDER, W., STEMMER, C., SATTELMAYER, T. AND WEIGAND, B. (2018). Fundamental technologies for the development of future space transport system components under high thermal and mechanical loads. In: *Proceedings of the 54nd AIAA/SAE/ASEE Joint Propulsion Conference*. Cincinnati, USA.

[3] RAHN, D., RIEDMANN, H. AND HAIDN, O. (2019). Extension of a non-adiabatic flamelet combustion model for composition predictions in thermal boundary layers. In: *Proceedings of the 8th European Conference for Aeronautics and Aerospace Sciences*. Madrid, USA.

[4] SILVESTRI, S., CELANO, M., SCHLIEBEN, G. AND HAIDN, O. (2016). Characterization of a multi-injector GOX/GCH4 combustion chamber. In: *Proceedings of the 52nd AIAA/SAE/ASEE Joint Propulsion Conference*. Salt Lake City, USA.

[5] SILVESTRI, S., CELANO, M., SCHLIEBEN, G., KIRCHBERGER, C. AND HAIDN, O. (2014). Characterization of a GOX-GCH4 single element combustion chamber. In: *Sonderforschungsbereich Transregio 40 – Summer Program Report 2014*.

[6] PERAKIS, N., STERNIN, A., ROTH, C. AND HAIDN, O. (2017). Heat transfer and combustion simulation of a 7-element GOX/GCH4 rocket combustor. In: *Sonderforschungsbereich Transregio 40 – Summer Program Report 2017*. Munich, Germany.

[7] SPALDING, D. (1971). Mixing and chemical reaction in steady confined turbulent flames. *Symposium (International) on Combustion*, **13**(1), 649–657. ISSN 0082-0784. DOI 10.1016/S0082-0784(71)80067-X.

[8] SPALDING, D. (1977). Development of the eddy-break-up model of turbulent combustion. *Symposium (International) on Combustion*, **16**(1), 1657–1663. ISSN 0082-0784. DOI 10.1016/S0082-0784(77)80444-X.

[9] SHVAB (2018). *Numerical investigation of the combustion process in a sub scale GCH4/GOX combustion chamber with the usage of the Eddy-Dissipation-Concept Model*. Semesterarbeit, TUM LTF. Munich, Germany.

[10] STANKOVIC, B., BELOSHEVIC, S., N.D., C., STOJANOVIC, A., TOMANOVIC, I. AND A.R., M. (2017). Specific aspects of turbulent flow in rectangular ducts. *Thermal Science*, **21**, 663–678. Papers presented at the Turbulence Workshop – International Symposium, held at the University of Belgrade, Faculty of Mechanical Engineering from August 31 to September 2, 2015.

[11] PRANDTL, L. (1927). Über die ausgebildete Turbulenz. International Congress for Applied Mechanics, Washington D.C., USA, NACA-TM-435.

[12] SLAVINSKAYA, N., ABBASI, M., STARKE, J., MIRZAYEVA AND A. HAIDN, O. (2016). Skeletal mechanism of the methane oxidation for space propulsion applications. In: *Proceedings of the 52nd AIAA/SAE/ASEE Joint Propulsion Conference*. Salt Lake City, USA.

[13] CELANO, M., SILVESTRI, S., BAUER, C., SCHLIEBEN, G. AND HAIDN, O. (2016). Comparison of a single and multi-injector GOX/GCH4 combustion chamber. In: *Proceedings of the 52nd AIAA/SAE/ASEE Joint Propulsion Conference*. Salt Lake City, USA.